



HAL
open science

An Experimental and Theoretical Study on the Effect of Silver Nanoparticles Concentration on the Structural, Morphological, Optical, and Electronic Properties of TiO₂ Nanocrystals

Faheem Ahmed, Mohammed Benali Kanoun, Chawki Awada, Christian Jonin,
Pierre-François Brevet

► To cite this version:

Faheem Ahmed, Mohammed Benali Kanoun, Chawki Awada, Christian Jonin, Pierre-François Brevet. An Experimental and Theoretical Study on the Effect of Silver Nanoparticles Concentration on the Structural, Morphological, Optical, and Electronic Properties of TiO₂ Nanocrystals. *Crystals*, 2021, 11 (12), pp.1488. 10.3390/cryst11121488 . hal-03460973

HAL Id: hal-03460973

<https://hal.science/hal-03460973>

Submitted on 1 Dec 2021

HAL is a multi-disciplinary open access archive for the deposit and dissemination of scientific research documents, whether they are published or not. The documents may come from teaching and research institutions in France or abroad, or from public or private research centers.

L'archive ouverte pluridisciplinaire **HAL**, est destinée au dépôt et à la diffusion de documents scientifiques de niveau recherche, publiés ou non, émanant des établissements d'enseignement et de recherche français ou étrangers, des laboratoires publics ou privés.

1 Article

2 An Experimental and Theoretical Study on the Effect of Silver 3 nanoparticles concentration on the Structural, Morphological, 4 Optical, and Electronic Properties of TiO₂ Nanocrystals

5 Faheem Ahmed^{1*}, Mohammed Benali Kanoun¹, Chawki Awada^{1*}, Christian Jonin² and Pierre –Francois Brevet²6 ¹ Department of Physics, College of Science, King Faisal University, P.O. Box 400, Al-Ahsa, 31982, Saudi Ara-
7 bia8 ² Institut Lumière Matière, Université de Lyon, UMR 5306 CNRS, Université Claude Bernard Lyon 1, 69622
9 cedex, Villeurbanne, France

10 * Correspondence: fahmed@kfu.edu.sa; cawada@kfu.edu.sa

11 **Abstract:** In this work, pure and silver (Ag)-loaded TiO₂ nanocrystals (NCs) with various concen-
12 tration of Ag were prepared by soft chemical route and the effect of Ag nanoparticles (NPs) on the
13 functional properties of TiO₂ was studied. X-ray diffraction (XRD) and Raman studies confirmed
14 that the synthesized product had single phase nature and high crystalline quality. The crystallite
15 size was decreased from 18.3 nm to 13.9 nm with the increasing in concentration of Ag in TiO₂ NCs.
16 FESEM micrographs showed that the pure and AgNPs-loaded TiO₂ have spherical morphology
17 and uniform size distribution with the size ranging from 20 to 10 nm. Raman scattering spectra of
18 pure and AgNPs-loaded TiO₂ revealed the characteristic mode that is related to the vibration of
19 oxygen atoms in TiO₂. Optical properties show the characteristics peaks of TiO₂ and the shifting of
20 the peaks position was observed by changing the concentration of Ag. The tuning of bandgap was
21 found to be observed with the increase in Ag, which could be ascribed to the synergistic effect
22 between silver and TiO₂ NCs. Density functional theory calculations are carried out for different Ag
23 series of doped TiO₂ lattices to simulate the structural and electronic properties. The analysis of the
24 electronic structures show that Ag loading induces new localized gap states around the Fermi level.
25 Moreover, the introduction of dopant states in the gap region owing to Ag doping can be conven-
26 nient to shift the absorption edge of pristine TiO₂ through visible light.

27 **Keywords:** TiO₂; Nanocrystals; Band-gap; XRD; Ag loading; Electronic structure
28

29 1. Introduction

30 Semiconductor-based photocatalysts have attracted great attention owing to their
31 potential applications in photocatalysts, water splitting for hydrogen production, and
32 renewable energy by converting sunlight to electricity or fuels [1,2]. Among these mate-
33 rials, TiO₂ is considered to be one such promising metal oxide because it possesses ex-
34 cellent physical and chemical properties, such as high oxidative power, long term stabil-
35 ility, non-toxicity, and low cost [3–5]. TiO₂ has a wide band gap [6] in which the absorption
36 coefficient is limited in the ultraviolet light region. Furthermore, photoexcited elec-
37 tron–hole pairs tend to recombine relatively easily in TiO₂ [7]. Both of these factors limit
38 possible applications in photocatalytic materials' design. Therefore, tuning the band gap
39 of TiO₂ to make it photosensitive to the visible-light region with low electron–hole re-
40 combination has become one of the most important goals in photocatalyst studies [8].

41 Doping TiO₂ with noble metal nanoparticles such as Pt, Ag, Pd, Au, and alloys is one
42 of the most effective approaches to improve the photocatalytic properties by visible light
43 harvesting and charge carrier separation simultaneously without crystal destruction in
44 TiO₂ [9, 10]. When metals and semiconductors are in contact, because of the lower Fermi

45 levels of metals, they can act as an electron reservoir suppressing the recombination rate,
46 thus extending the life-time of charge carriers and significantly enhancing the
47 photocatalytic performance [11,12]. Among the noble metals, silver nanoparticles (Ag
48 NPs) has been shown to be an active catalytic element and has been applied to various
49 catalysts due to its unique physical, chemical, electronic and optical properties [13-15].
50 The presence of Ag NPs in vicinity of TiO₂ NCs also increases its photocatalytic efficiency
51 via the interfacial charge transfer (IFCT) that occurs effectively towards the Ti-Ag-O
52 phase and the presence of oxygen vacancies [16]. The presence of surface plasmon reso-
53 nance of Ag NPs during the visible irradiation drive the electron from metallic NPs to
54 TiO₂ or the reverse way and in turn improve light harvesting [17, 18].

55 Various methods to fabricate Ag doped TiO₂ have been reported. For example, some
56 studies have used chemical reduction method by doping Ag⁺ into TiO₂ NPs [16, 19]. Yang
57 et al, used photo-reduction method of silver nitrate (AgNO₃) by using TiO₂ NPs under
58 UV light [20]. Zhou et al. fabricated Ag/Ag-doped TiO₂ used modified sol-hydrothermal
59 method with the assistance of NaOH additive [21]. Al Suliman et al. synthesized Ag/TiO₂
60 nanorods by chemical reduction route by doping Ag⁺ into Ti Sheet at high temperature
61 [22]. Although, we use in this work the chemical route to fabricate Ag doped TiO₂ NCs.
62 Theoretically, First-principles calculations based on density-functional theory (DFT) have
63 provided significant contributions towards understanding the physical and chemical
64 processes involved in photocatalysis [23-25]. Numerous theoretical investigations on
65 TiO₂ photocatalysts have been performed during recent decades. Moreover, they have
66 been also reviewed to support the experimental results [26-35]. The electronic structures
67 of metal/TiO₂ interfaces have previously been studied by DFT calculations [36]. The effect
68 of the formation of oxygen vacancies in the TiO₂ layer near the interface has also been
69 investigated [36–40]. An important progress in the theory of catalysis has been made by
70 Hammer and Norskov, [41] who suggested that trends in reactivity on a metal surface
71 can be understood in terms of the energy of hybridization between the bonding and an-
72 ti-bonding adsorbate states and the metal d-bands.

73 In this work, we report the chemical synthesis of **AgNPs-loaded TiO₂** and study the
74 effect of Ag nanoparticles on the structural, optical and electronic structure properties of
75 TiO₂ to explore the possibility of utilizing the prepared nanomaterials for photocatalytic
76 applications. The results showed that by simply altering the concentration AgNPs in TiO₂
77 matrix resulted in tuning of bandgap of TiO₂ which could be beneficial for the enhance-
78 ment in photocatalytic activity. The theoretical studies were conducted to investigate the
79 structural, electronic and optical properties using the first-principles calculation method.
80 This leads to determine of the band gap change and allows for an investigation of the
81 structure/property relations in this **AgNPs-loaded TiO₂**.

82 2. EXPERIMENTAL AND COMPUTATIONAL METHODS

83 2.1. Experimental details

84 2.1.1. Synthesis of **AgNPs-loaded TiO₂**

85 For the synthesis of pure and Ag **loaded** (1%, 2%, 5%, 10%, and 19%) TiO₂
86 nanocrystals (TAg 0, TAg 1, TAg 2, TAg 5, TAg 10 and TAg 19), 0.1 M TiO₂ nanoparticles
87 were dissolved in 100 mL deionized water. The solution was then stirred on magnetic
88 stirrer for 1 hour. Required volume of AgNO₃ (0.1 M) solution was added to the existing
89 sol. Reduction of Ag⁺ was carried out by drop-wise addition of 25 mL ascorbic acid
90 (0.02 M), until a color change from colorless to brownish was noted. **This solution (silver
91 nitrate and ascorbic acid) was heated in microwave at a power of 450 W for few minutes
92 to complete the reaction which resulted in AgNPs-loaded TiO₂. Centrifuging and drying
93 the prepared samples was carried out, the final product was then grinded using mortar
94 and the product was then used for further characterizations.**

95 2.2.2. Characterizations

XRD was used to determine the phases of the product. XRD measurements on different powders were performed using Philips X'pert MPD 3040 x-ray powder diffractometer operated at 40 kV and 30 mA with CuK α (1.541Å) radiation. The UV-Visible spectrometer (Agilent 8453) was used to record the absorption spectrum of AgNps-loaded TiO₂ nanocrystals in the range of 200 to 800 nm of wave length using the combination of Tungsten and Deuterium lamp. FTIR (Perkin Elmer; Spectrum Two) was used to study the structural studies of the prepared product. Morphologies of the samples were studied using field emission scanning electron microscopy (FESEM; JEOL JSM 7600 F). High resolution transmission electron microscopy (HRTEM) images of the sample were obtained using images were obtained using a FE-TEM (JEOL/JEM-2100F version) operated at 200 kV. The structure of the prepared samples was analyzed by Raman microscope (HORIBA; LabRAM HR800, France SAS) at room temperature and an ambient atmosphere with a He-Ne wavelength laser of 633 nm and power of 20 mW.

2.2. Computational details

All calculations were carried out using the framework of the density functional theory (DFT) within the local combination of the atomic orbitals (LCAO) approach as implemented in the Quantum Atomistix ToolKit (quantumATK) [42] package. The Perdew, Burke, Ernzerhof (PBE) with the generalized gradient approximation (GGA) to the exchange correlation functional is employed [43]. The norm-conserving PseudoDojo [44] pseudopotential was chosen for characterizing the interaction between ion nuclei, and the valence electrons. The computation of self-consistent field (SCF) was iterated until the difference of total energy less than 10⁻⁶ Ha was completed. The structures were fully optimized by using the limited-memory Broyden–Fletcher–Goldfarb–Shanno algorithm, with force on each atom site fewer than 0.05 eV/Å. For the geometry optimization, a 4 × 4 × 3 Monkhorst-Pack [45] k-grid is used, and for electronic property calculations, a 10 × 10 × 8 grid is used. The electronic and optical properties are calculated using a more accurate Heyd–Scuseria–Ernzerhof hybrid functional (HSE06) [46, 47].

3. Results and discussion

3.1. Structural properties

3.1.1. X-ray diffraction analysis

XRD patterns were studied to illustrate the structure and phase composition of as-synthesized materials. Figure 1 displays the results of XRD of pure TiO₂ and AgNps-loaded TiO₂ nanocrystals synthesized by above described method. From the XRD pattern, it is observed that the diffraction peaks at 2 θ angles 25.3, 37.9, 48.05, 53.9, 55.06, 62.4, 68.76, 70.3, 75.06, 78.67 corresponding to the crystal planes (101), (004), (105), (211), (204), (116), (215), (206) belong to the fundamental anatase structure of TiO₂ (JCPDS card no. 21-1272). Further it can be observed that the shape of the peaks appears clear and sharp and no impurity peaks are there in these patterns which indicates pure form of TiO₂. In addition, some of the peaks marked by (*) belong to the crystal planes of silver (JCPDS card no. 04-0783). The intensities of these peaks increase with the increasing concentration of Ag in TiO₂ expect the 10 % concentration of silver where the intensity is higher than 19%, this difference could be due to the slower agglomeration rate of silver nanoparticles and with the more excess of silver cations. The crystallite size of all the prepared samples were calculated by using the Debye Scherrer formula which is given below [48]:

$$D = \frac{k\lambda}{\beta \cos\theta} \quad (1)$$

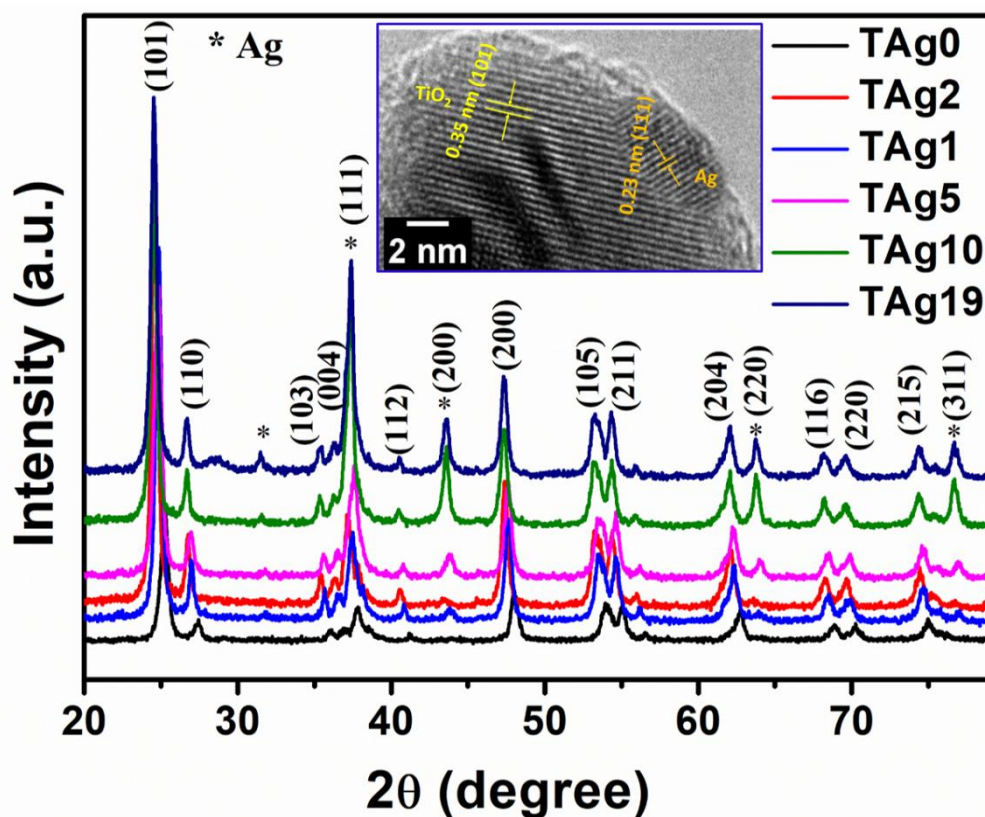


Figure 1. XRD patterns of pure and AgNPs-doped TiO₂ nanocrystals. Inset shows HRTEM image of AgNPs-loaded TiO₂.

where the letters have their usual meaning, k is a constant, λ is a wavelength of x ray used, β is the FWHM parameter and θ is the diffraction angle. It has been found that the crystallite size decreases with the increasing concentration of Ag in TiO₂ nanocrystals. It has been found that the crystallite size decreases with the increasing concentration of Ag in TiO₂ nanocrystals, these results are in good agreement with the previous work [49]. The crystallite size of pure and AgNPs-loaded TiO₂ nanocrystals was found in the decreasing order as 18.30, 17.52, 17.45, 17.35, 14.57, 13.91 nm with 0%, 1%, 2%, 5%, 10%, and 19% Ag, respectively. Inset of Fig. 1 shows the HRTEM image of AgNPs-loaded TiO₂ (2%) in which clear interplanar spacing of 0.36 nm corresponds to (101) plane of TiO₂ and 0.23 nm corresponds to (111) plane of Ag, respectively could be seen. Additionally, the attachment of AgNPs on the surface of TiO₂ is also evident from the HRTEM image.

3.1.2. FTIR analysis

Figure 2 displays the FTIR spectra of pure and AgNPs-loaded TiO₂ nanocrystals. It confirms that the strong absorption peaks of pure TiO₂ and AgNPs-loaded TiO₂ at 3396, 1684, 1619 and 1420 cm⁻¹ have identical behavior, which is possibly due to hydrogen bonded surface hydroxyl groups and OH of adsorbed water molecules [50]. Further, the vibration peak 1630 cm⁻¹ can be ascribed to the O–H bond. The peak at 1411 cm⁻¹ can be ascribed to the alcohol group which occurs due to the addition of ethanol solution while washing the samples. The strong absorption peak around ~450 cm⁻¹ describes the formation of pure and AgNPs-loaded TiO₂ nanocrystals. Furthermore, with the increase in concentration of Ag in TiO₂, there is a shift in the characteristics peak (~450 cm⁻¹) to-

wards higher wavenumber as shown in the zoomed area of marked region in Fig. 2, and the occurrence of new peaks correspond to AgNPs (~1400 cm⁻¹) were observed.

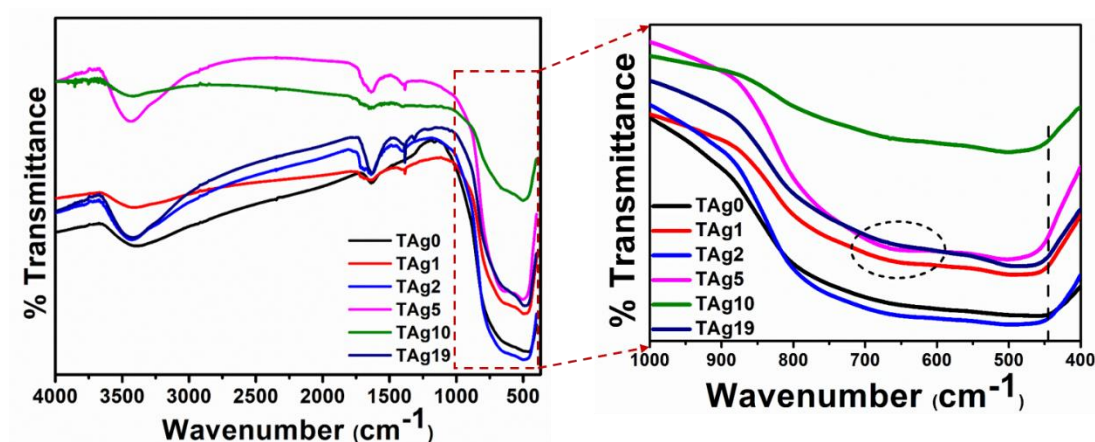


Figure 2. FTIR spectra of pure and Ag doped TiO₂ nanocrystals, and zoomed area of selected region in FTIR spectra.

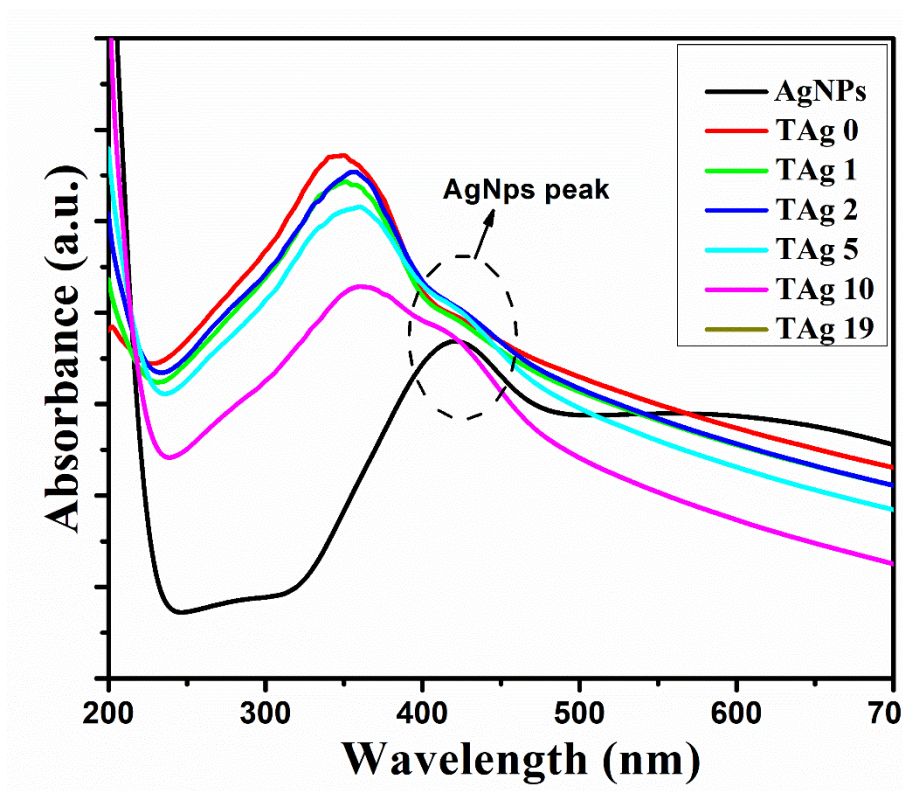
3.2. Optical properties

The UV-Vis absorption spectra of the pure and AgNPs-loaded TiO₂ nanocrystals are shown in Fig. 3 (a). As TiO₂ belongs to the wide band gap semiconductor and hence it doesn't show any absorption peak in the visible region. The obtained absorption spectra show that the maximum absorption is ~ 340-350 nm which is due to the strong interaction between O 2p → Ti 3d charges. In order to confirm the presence of AgNPs, UV-Vis of AgNPs alone is shown which depicts a clear absorption peak at ~ 421 nm corresponds to the metallic Ag. It is observed that the intensity of absorption decreases with increasing Ag concentration in TiO₂. This occurs due to the attachment of Ag nanoparticles to the TiO₂ surface. The Ag nanoparticles show much higher absorption coefficient in the visible range than pure TiO₂. The absorption intensity of the pure and AgNPs-loaded TiO₂ nanocrystals has been calculated using the relation

$$I = I_0 * e^{-\alpha t} \quad (2)$$

Whereas, the absorption coefficient (α) is calculated by the formula

$$\alpha = \frac{2.303 * A}{t} \quad (3)$$



185 **Figure 3. (a).** UV-Vis absorption spectra of pure and AgNPs-loaded TiO₂ nanocrystals.

186
187 Figure 3 (b) displays the band gap of pure and Ag doped TiO₂ nanocrystals. The
188 energy band gaps were calculated using Tauc's relation and is given by [51]:

$$\alpha h\nu = B(h\nu - E_g)^n \quad (4)$$

189 where $n=2$ for indirect band gap semiconductor. The tuning of band gap was found
190 to be 3.01 eV, 2.98 eV, 2.95 eV, 2.91 eV, 2.71 eV and 2.63 eV for 0%, 1%, 2%, 5%, 10%, and
191 19%, respectively. It was observed that the band gap was slightly decreased with 1%
192 Ag, 2% Ag, and 5% Ag in TiO₂, while, with higher concentration of Ag such as 10%, and
193 19%, resulted in the abrupt decrease of band gap as compared to pure TiO₂ (see Fig. 3 (b)
194 and 3 (c)). Therefore, the optimum concentration of Ag in TiO₂ to make it visible light ef-
195 ficient could be taken as 5% Ag which could be extend to 10% with decreased bandgap,
196 thus increased visible light absorption.

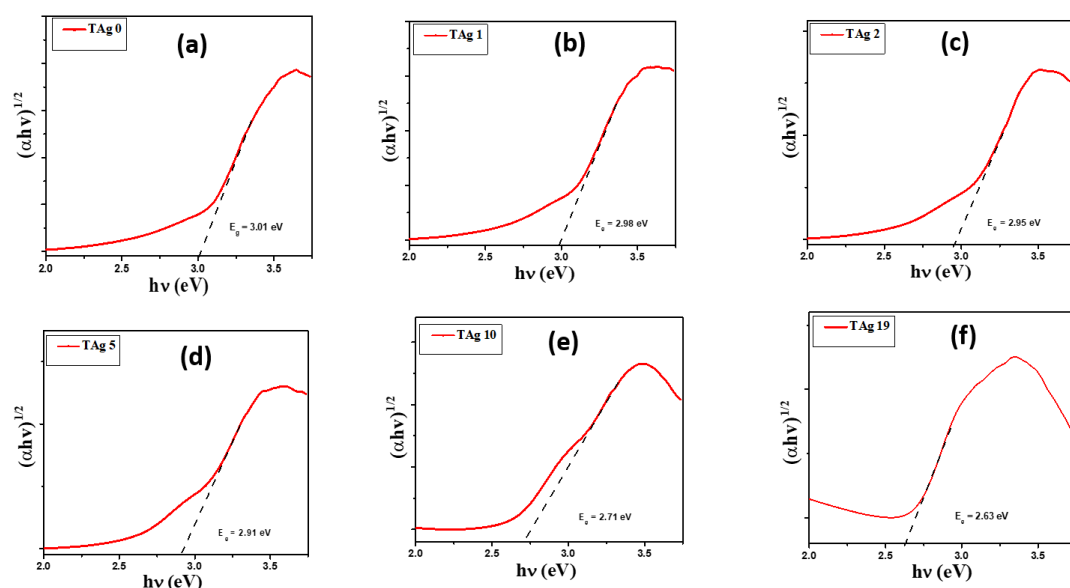


Figure 3. (b). Band gap determination of pure and AgNPs-loaded TiO₂ nanocrystals.

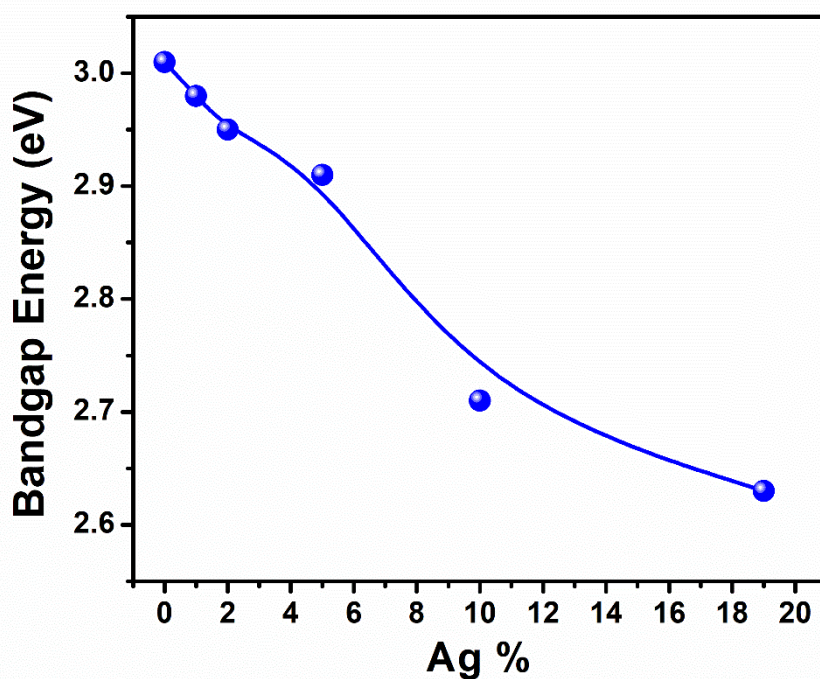


Figure 3. (c). Plot of Band gap as a function of Ag% for pure and AgNPs-loaded TiO₂ nanocrystals.

3.3. Raman Analysis

Figure 4 shows the Raman spectra of pure and AgNPs-loaded TiO₂ nanocrystals. The pure TiO₂ shows an intense Raman peak at 145 cm⁻¹, which can be assigned to the Eg optical Raman mode of anatase TiO₂. The other Raman peaks at 196 cm⁻¹, 394 cm⁻¹, 512 cm⁻¹ and 636 cm⁻¹ were assigned to E_g, B_{1g}, A_{1g} and E_{1g} Raman modes of anatase TiO₂ respectively. In the case of AgNPs-loaded TiO₂ nanocrystals, all the Raman peaks of TiO₂ have been observed, while no Raman active peak from Ag was observed due to the crystal symmetry of Ag [19, 52].

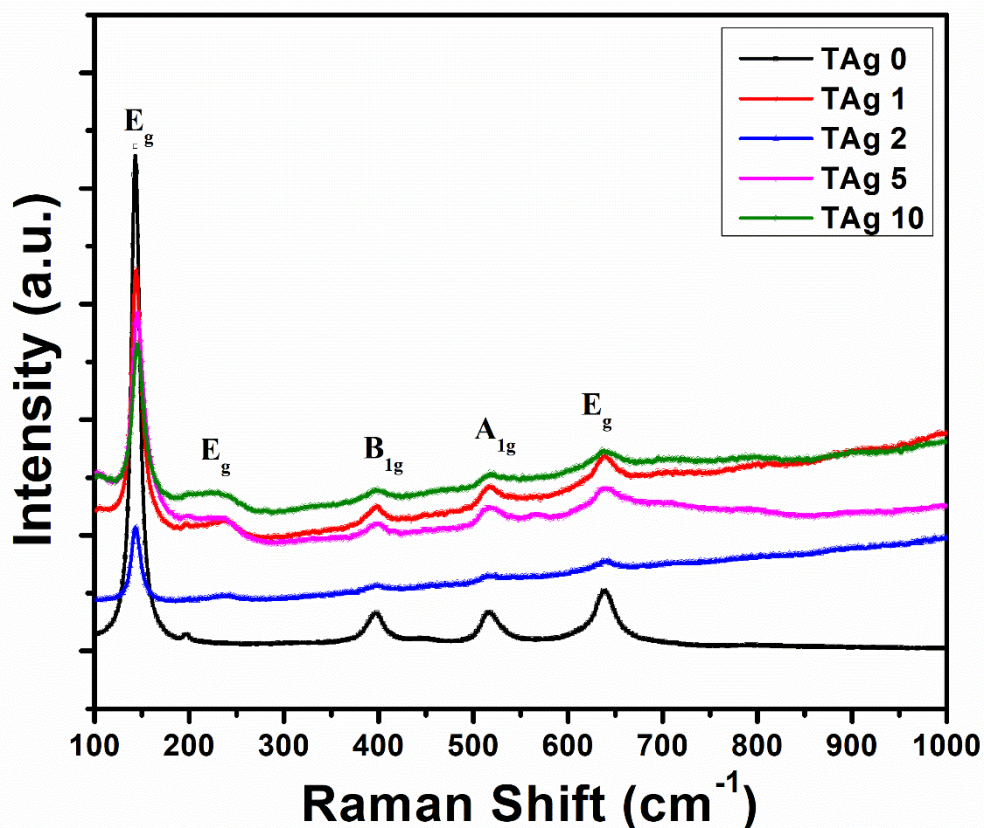


Figure 4. Room temperature Raman spectra of pure and AgNPs-loaded TiO₂ nanocrystals.

3.4. Morphological studies

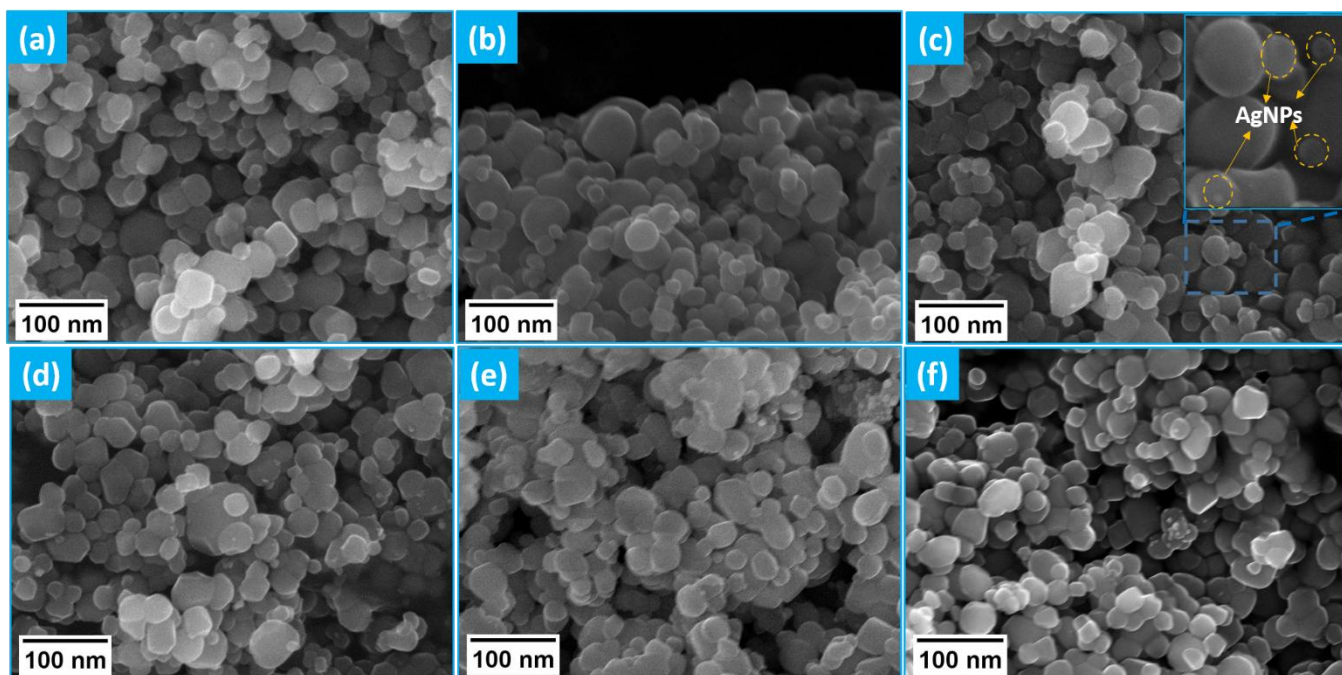


Figure 5. FESEM images of (a) pure TiO₂, (b) 1% AgNPs-loaded TiO₂, (c) 2% AgNPs-loaded TiO₂, (d) 5% AgNPs-loaded TiO₂, (e) 10% AgNPs-loaded TiO₂, and (f) 19% AgNPs-loaded TiO₂. Inset of (c) shows the zoomed area of selected region in which AgNPs are attached the surface of TiO₂.

Fig. 5 displays the FESEM images of synthesized pure and AgNPs-loaded TiO₂ nanocrystals under similar experimental conditions. Fig. 5(a) shows the FESEM micrograph of pure TiO₂ sample where the particles are well distributed all over the surface and exhibited well defined regular spherical structures. The spherical shape particles have almost uniform size in the range of 20-25 nm. The morphology of AgNPs-loaded TiO₂ can be clearly seen from Fig. 5(b)–(f), and it was observed that the particle size decreased with the increasing concentration of Ag nanoparticles in TiO₂. More specifically, Fig. 5(b) shows the morphology of sample synthesized using 1% AgNPs-loaded TiO₂ nanocrystals which has particle size of 18-22 nm. When the concentration of Ag further increased to 2%, the particle size reduced to 18-20 nm (see Fig. 5(c)). Further increase in Ag concentration to 5% in TiO₂, reduction of particle size of 17-19 nm can be observed. Upon increase in the concentration of Ag to 10% and 19%, the particles size was decreased to 15-18 nm (see Fig. 5(e)), and 14-19 nm (see Fig. 5(f)), respectively. The reduced size of the nanoparticles might be related to the effect of confined electrons, which hinders the interaction of surface Plasmon resonance at visible light, such as was noted by UV-vis and Raman spectroscopy. This phenomenon can be associated with electronic barrier sets for Ag NPs with very small sizes, e.g. diameters < 20 nm, such as was explained by Tsivadze A, et al. [53]. Interestingly, the anchored Ag nanoparticles on the surface of TiO₂ could be seen for the samples doped with Ag nanoparticles (Fig. 5(b)–(f)) which further confirms the successful attachment of Ag nanoparticles on the surface of TiO₂ nanocrystals.

3.5. Electronic properties

We started by performing a structural analysis of defect free TiO₂ prior to investigating the defects using first principles calculations. The anatase structure is the most common polymorphs of TiO₂ which is hexagonal (the space group I4₁/amd), as shown in Fig. 6. The optimized lattice parameters, $a = 3.782 \text{ \AA}$, $c = 9.496 \text{ \AA}$, show a fair agreement with the experimentally reported values ($a = 3.7842 \text{ \AA}$, $c = 9.5146 \text{ \AA}$) [54]. To construct configurations doped with TiO₂, a $2 \times 2 \times 1$ supercell consisting of 48 atoms was used, as shown in Figure 6. Substitutional defects are induced in the supercell to model the different doped systems [55]. Three types of doping configurations are modeled, including one substitutional Ag at Ti site (equivalent to 6.25% Ag concentration), two substitutional Ag at Ti sites (equivalent to 12.5% Ag concentration), and three substitutional Ag at Ti sites at (equivalent to 18.75% Ag concentration). The incorporation of Ag dopants into the anatase lattice at Ti sites shows that a - and c -lattice parameters change a little compared to those of pristine TiO₂ (Table 1). This difference occurs from the tetragonal lattice distortion after the incorporation of Ag dopants. The optimized Ti–O and O–O average bond lengths of pure TiO₂ are 1.960 and 2.47 Å, respectively, which are rather close with the experimental measurements [54] and theoretical values [56-58]. For the introduction of single Ag impurity, the process decreases the Ti–O and increases O–O bond distance because of the crystalline structure distortion. Our results show that Ag doping shows a long-range impact on the system, in which all lengths of interatomic bond are changed [59]. A similar feature is observed for two and three Ag doping.

Table 1. lattice parameters, a , c , volume, V , and average bond lengths (Å) of pure and doped anatase TiO₂.

	a (Å)	c (Å)	V (Å ³)	Ti–O	O–O	O–Ag
Pristine	3.782	9.496	543.34	1.960	2.47	-
Ag(6.25%)	3.800	9.528	550.40	1.950	2.50	2.030
Ag(12.5%)	3.818	9.572	557.08	1.951	2.48	2.064
Ag(18.75%)	3.845	9.586	561.11	1.950	2.478	2.020

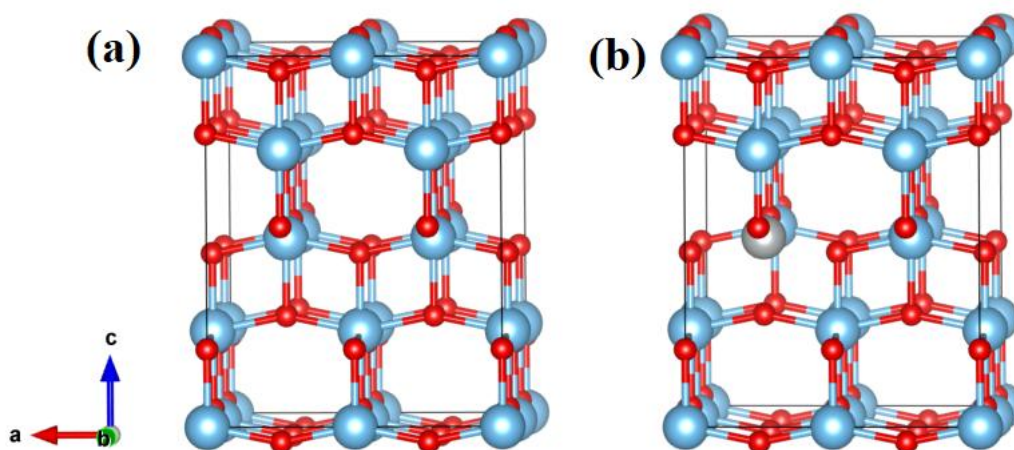


Figure 6. The optimized geometry structures of $2 \times 2 \times 1$ supercell model of anatase undoped and (b) Ag doped TiO₂. The blue, red and gray spheres represent Ti atoms, O atoms, and Ag atom, respectively.

Band structure plots for pristine and Ag doped anatase TiO₂ with different concentrations are shown in Figure 7. For pristine anatase TiO₂, our computed band gap energy of 3.16 eV with HSE06 functional agrees well with the experimental value (3.01 eV) in which the top of the valence band is located near Γ -X points while the bottom of the conduction band is located at Γ point. When substituting one Ti by an Ag atom, the band structure of the host TiO₂ is perturbed by adding an acceptor levels above valence band edge, as illustrated in Fig. 7(b). The induced impurity state near the valence band edge is also clearly appearing in the corresponding density of states (DOS), reflecting the achievement of the p-type states. Introduction of impurity states in the gap region owing to Ag doping may be convenient to shift the absorption edge of pristine TiO₂ into visible light. For two Ag doping at two Ti sites in TiO₂ supercell, an increased amount of impurity energy levels is appeared in band gap just above the valence band edge, which may facilitate in transferring excited electrons by visible-light to the conduction band (see Fig. 7c). With increasing dopant concentration by replacing three Ti atoms by three Ag atoms, it shows from Figure 7d that more impurity states are created near the Fermi level and above valence band maximum (VBM). All these findings show that increasing Ag dopant concentration in TiO₂ supercell may reveal greater p-type behavior than the single Ag doped system which might be practical in absorbing visible light low-energy photons. To explain the modifications in the band structures, the total and partial DOS are calculated using the HSE06 functional and displayed in Fig. 7. The analysis of DOS of pure anatase TiO₂ shows that the conduction band minimum is mainly made by Ti 3d states whereas the valence band maximum is dominated by the contribution of O 2p states. From Figure 7b, the Ag doping introduces acceptor states in which the contribution of Ag 4d states is larger compared with O 2p states, indicating the occurrence of the O 2p - Ag 4d hybridization. Moreover, the VBM and conduction band maximum (CBM) shift to higher energies. With Ag incorporation concentration rising, more defect states are added. It is noticed that the VBM and CBM of two and three Ag doping configurations keep nearly at the same position. It is found that with increasing substitution concentration, the number of defect states incorporated in the gap region increases with a wide distributed above the VBM.

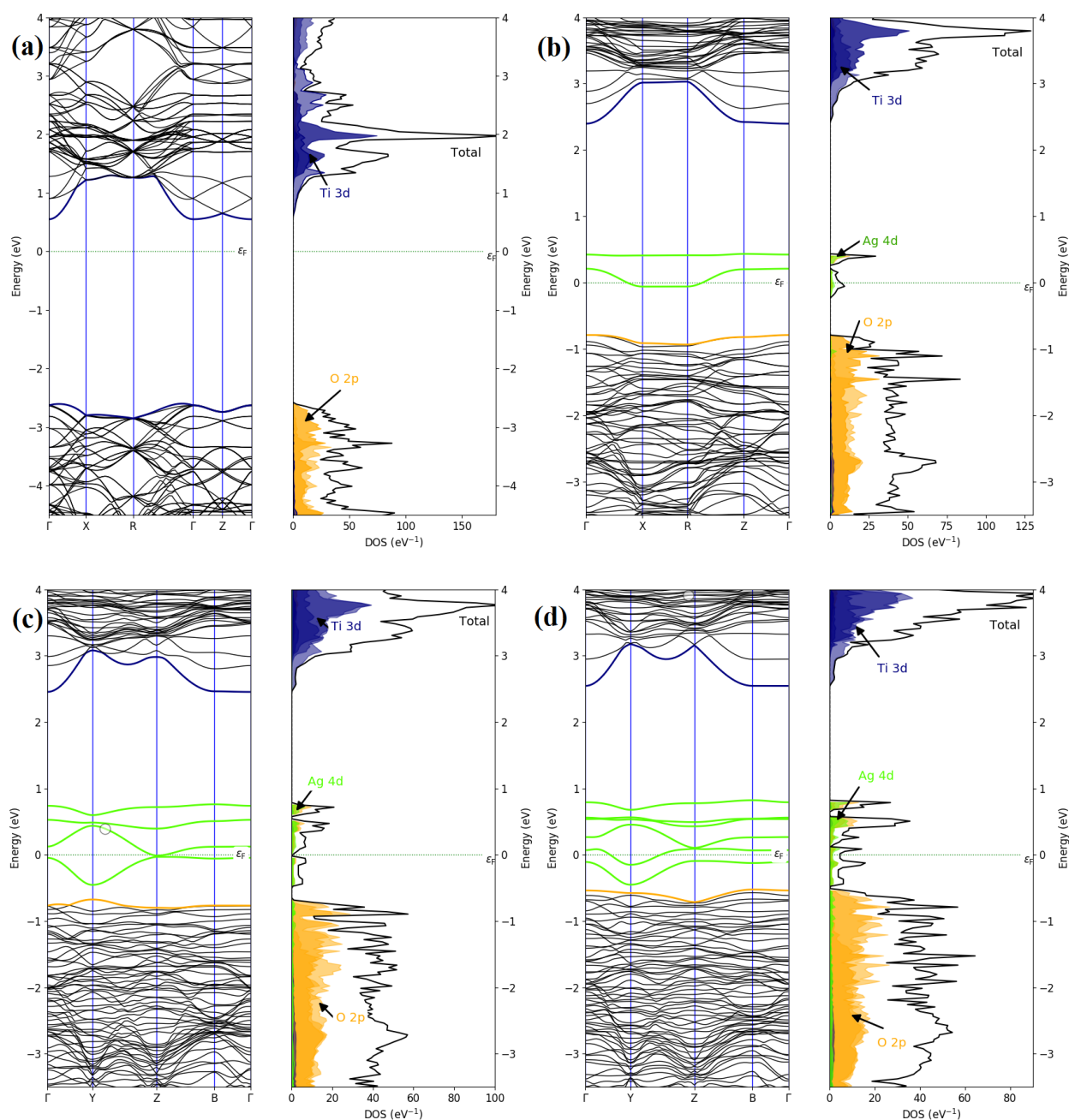


Figure 7. Calculated Band structures and total and partial DOS of (a) pristine (b) Ag(6.25%) doped TiO₂, (c) Ag(12.5%) doped TiO₂ and (d) Ag(18.75%) doped TiO₂.

To estimate the optical harvesting ability, the absorption coefficients are computed at HSE06 levels for undoped and doped TiO₂ at different concentrations, as illustrated Fig. 8. The spectrum of TiO₂ reveals the appearance of high intensity resonant peaks in the ultraviolet range and displays no absorption response in the visible region. Doping Ag into TiO₂ structure modified the absorption spectrum of pristine TiO₂. It shows a good optical absorption property in the visible region. Note that there is a strong absorption peak in UV region at 220 nm and another absorption peak at about 520 nm in the visible light range. Interestingly, the improved absorption is ascribed to the photons absorptions because of the electron excitation from valence band edge to the Ag 4d gap states, inducing significant red shift, corresponding to the absorption at 520 nm. This result is consistent with the previous theoretical results [56]. With the increase of Ag substitution concentration, synergistic effect of Ag(12.5%) and Ag(18.75%) doping induces more impurity Ag 4d gap states, which lead to the improvement of the visible-light photocatalytic

ability. Therefore, the absorption of visible- and UV-light is highly enhanced in Ag(18.75%) doping compared with the pure, and other doping configurations.

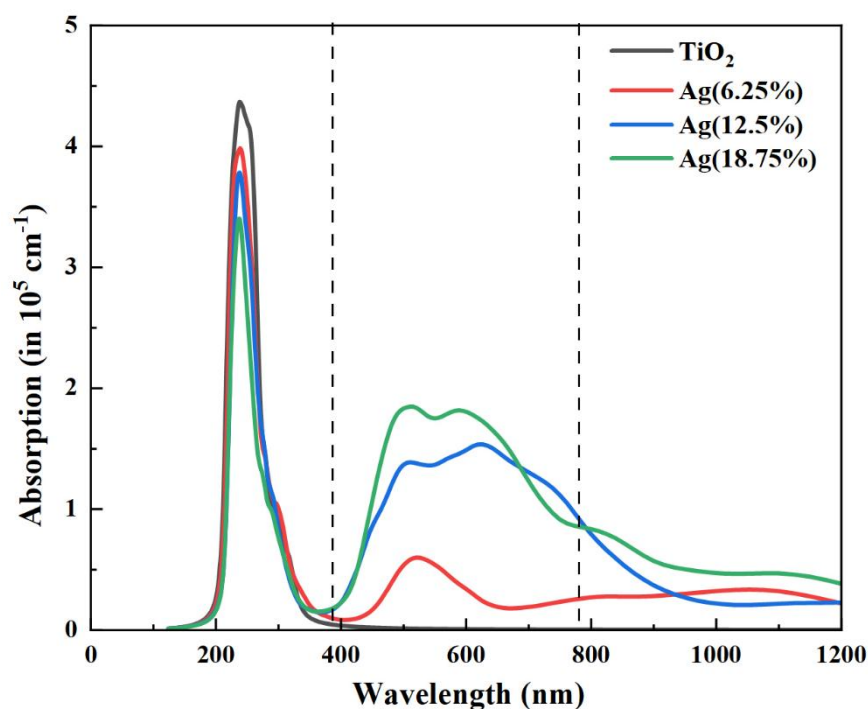


Figure 8. Calculated Absorption coefficient spectra of Ag doped TiO₂ as compared with those of pristine TiO₂.

4. Conclusion

In summary, pure and AgNPs-loaded TiO₂ nanocrystals with various concentration of Ag nanoparticles were successfully prepared. XRD and Raman studies confirmed that single phase nature and high crystalline quality of the product. In the nanocomposites, the presence of both the Ag and TiO₂ phases revealed the formation of loaded TiO₂ with Ag NPs. It was observed that the size was tuned with the Ag concentration in TiO₂. FTIR studies showed the characteristics bands of TiO₂ and Ag without any additional bands features. Optical properties studied by UV-Vis spectroscopy show the characteristics peaks of TiO₂ and Ag, and the shifting of the peaks position was observed by changing the concentration of Ag. The tuning of bandgap was found to be observed with the increase in Ag, which could be ascribed to the synergistic effect between AgNPs and TiO₂ NCs. Morphological characterizations by using FESEM show that the particles size was reduced with the increase of Ag in the TiO₂, however keeping the shape of the nanoparticles unchanged. First principles calculations are performed for various Ag configurations of doped TiO₂ structures to calculate the structural and electronic properties. The analysis of the electronic structures show that Ag doping induces new localized gap states around the Fermi level. Moreover, the incorporation of dopant states in the gap region owing to Ag doping can be convenient to shift the absorption edge of pristine TiO₂ through visible light.

Acknowledgements: The authors extend their appreciation to the Deputyship for Research & Innovation, Ministry of Education in Saudi Arabia for funding this research work through the project number (1063).

Conflicts of Interest: The authors declare that they have no competing interests.

Author Contributions: Conceptualization, Faheem Ahmed, Mohammed Benali Kanoun, and Chawki Awada; Data curation, Faheem Ahmed, Mohammed Benali Kanoun; Formal

analysis, Faheem Ahmed, Mohammed Benali Kanoun; Funding acquisition, Chawki Awada; Methodology, Faheem Ahmed, Chawki Awada; **Computational methodology, Mohammed Benali Kanoun**, Resources, Chawki Awada; Visualization, Mohammed Benali Kanoun, Chawki Awada; Writing – original draft, Faheem Ahmed, Mohammed Benali Kanoun; Writing – review & editing, Chawki Awada, Christian Jonin, Pierre –Francois Brevet.

References

- [1] Khan, S. U. M.; Al-Shahry, M.; Ingler, W. B., Jr. 2002, 297, 2243–2245.
- [2] Chen, X.; Mao, S. S. Chem. Rev. 2007, 107, 2891–2959.
- [3] Y. Lin, Z. Jiang, C. Zhu, X. Hu, X. Zhang, H. Zhu and J. Fan, Appl. Phys. Lett., 2012, 101, 062106.
- [4] W. J. Yin, H. Tang, S. H. Wei, M. M. Al-Jassim, J. Turner and Y. Yan, Phys. Rev. B: Condens. Matter Mater. Phys., 2010, 82, 045106.
- [5] Liu, L.; Jiang, Y.; Zhao, H.; Chen, J.; Cheng, J.; Yang, K.; Li, Y. ACS Catal. 2016, 6, 1097–1108
- [6] M.D. Hernandez-Alonso, F. Fresno, S. Suarez, J.M. Coronado, Energy Environ. Sci. 2 (2009) 1231–1257.
- [7] Y. Gai, J. Li, S. S. Li, J. B. Xia and S. H. Wei, Phys. Rev. Lett., 2009, 102, 036402.
- [8] J. Chang, Z.-Y. Jiang, Z.-Y. Zhang, Y.-M. Lin, P.-L. Tian, B. Zhou, L. Chen Appl. Surface Science 484 (2019) 1304–1309
- [9] K. Wilke and H. Breuer, J. Photochem. Photobiol., A, 1999, 121,49–53.
- [10] S. W. Verbruggen, M. Keulemans, M. Filippousi, D. Flahaut, G. V. Tendeloo, S. Lacombe, J. A. Martens, Si. Lenaerts, Applied Catalysis B: Environmental 156–157 (2014) 116–121.
- [11] W. Choi, A. Termin and M. R. Hoffmann, J. Phys. Chem., 1994, 98, 13669–13679.
- [12] Jenny Schneider, Masaya Matsuoka, Masato Takeuchi, Jinlong Zhang, Yu Horiuchi, Masakazu Anpo, and Detlef W. Bahnemann, Chem. Rev. 2014, 114, 9919–9986.
- [13] Zhang, H.; Liang, C.; Liu, J.; Tian, Z.; Wang, G.; Cai, W. Defect-Mediated Formation of Ag Cluster-Doped TiO₂ Nanoparticles for Efficient Photodegradation of Pentachlorophenol. *Langmuir* 2012, 28, 3938–3944, doi:10.1021/la2043526.
- [14] Subrahmanyam, A.; KP, B.; Rajesh, P.; Kumar, K.J.; MR, K. Surface modification of sol gel TiO₂ surface with sputtered metallic silver for Sun light photocatalytic activity: Initial studies. *Sol. Energy Mater. Sol. Cells* 2012, 101, 241–248, doi:10.1016/j.solmat.2012.01.023.
- [15] Li, Y.; Ma, M.; Chen, W.; Li, L.; Zen, M. Preparation of Ag-doped TiO₂ nanoparticles by a miniemulsion method and their photoactivity in visible light illuminations. *Mater. Chem. Phys.* 2011, 129, 501–505, doi:10.1016/j.matchemphys.2011.04.055.
- [16] Devipriya Gogoi, Ashutosh Namdeo, Animes Kumar Golder, Nageswara Rao Peela, international journal of hydrogen energy 45 (2020) 2729–2744.
- [17] L. Liu, S. Ouyang and J. Ye, Angew. Chem., 2013, 125,6821–6825; (b) P. Wang, B. Huang, Y. Dai and M.-H. Whangbo, Phys. Chem. Chem. Phys., 2012, 14, 9813–9825.
- [18] M. L. de Souza, D. P. dos Santos and P. Corio, RSC Adv., 2018, 8, 28753
- [19] Z. V Quiñones-Jurado, M. Ángel Waldo-Mendoza, H Marcelo Aguilera-Bandin1, Edgar Giovanni Villabona-Leal, Elsa Cervantes-González4, Elías Pérez3, Silver Nanoparticles Supported on TiO₂ and Their Antibacterial Properties: Effect of Surface Confinement and Nonexistence of Plasmon Resonance, Materials Sciences and Applications, 2014, 5, 895-903
- [20] L. Yang, Q Sang, J. Du, M. Yang, X. Li, Y. Shen, X. Han, X. Jiang and B. Zhao, Phys.Chem.Chem.Phys., 2018, 20, 15149.
- [21] L. Zhou, J. Zhou, W. Lai, X. Yang, J. Meng, L. su, C. Gu, T. Jiang, E. Y. B. Pun, L. Shao, L. Petti, X. W. Sun, Z. Jia, Q. Li, J. Han, P. Mornile, NATURE COMMUNICATIONS | (2020) 11:1785.
- [22] N. Al Suliman, C. Awada, A. Alshoaibi and N. M. Shaalan, Crystals 2020, 10, 1024.
- [23] Y. Gai, J. Li, S.-S. Li, J.-B. Xia and S.-H. Wei, Phys. Rev. Lett., 2009, 102, 036402.
- [24] F. Wang, C. Di Valentin and G. Pacchioni, J. Phys. Chem. C, 2012, 116, 8901–8909.
- [25] M. M. Islam, M. Calatayud and G. Pacchioni, J. Phys. Chem. C, 2011, 115, 6809–6814.
- [26] A. Kubacka, M. Fernández-García and G. Colon, Chem. Rev., 2012, 112, 1555–1614.
- [27] V. E. Henrich, Prog. Surf. Sci., 1995, 50, 77–90.
- [28] R. Daghrir, P. Drogui and D. Robert, Ind. Eng. Chem. Res., 2013, 52, 3581–3599.
- [29] H. Park, Y. Park, W. Kim and W. Choi, J. Photochem. Photobiol., C, 2013, 15, 1–20.
- [30] R. Shwetharani, M. Sakar, C. A. N. Fernando, V. Binias and Sci. Technol., 2019, 9, 12–46
- [31] Y. Nam, J. H. Lim, K. C. Ko, J. Y. Lee J. Mater. Chem. A, 2019, 7, 13833
- [32] Y. Lin, Z. Jiang, C. Zhu, X. Hu, X. Zhang, H. Zhu, J. Fand, S. H. Linbe, J. Mater. Chem. A, 2013, 1, 4516
- [33] M. Niu, D. Cheng, D. Cao, J. Phys. Chem. C 2013, 117, 15911–15917
- [34] X. Zhou, H. Dong, ChemCatChem 2019, 11, 3688–3715
- [35] A. V. Vorontsov, H. Valdés, P. G. Smirniotis, Y. Paza, J Chem Technol Biotechnol 95, 2750-2760 2020
- [36] T. Tamura, S. Ishibashi, K. Terakura and H. Weng, Phys. Rev. B 2009, 80, 195302.
- [37] N. Shahzad, A. Hussain, N. Mustafa, N. Ali, M. B. Kanoun, S. Goumri-Said, First principles study of the adsorption and dissociation of H₂S on TiO₂ anatase (001) surfaces. RSC Advances, 6, 7941-7949 (2016).
- [38] K. Okazaki, Y. Morikawa, S. Tanaka, K. Tanaka and M. Kohyama, Phys. Rev. B 2004, 69, 235404.
- [39] I. Marri and S. Ossicini, Solid State Commun., 2008, 147, 205–207.

- [40] A. Boonchun, N Umezawa, T. Ohno, S. Ouyanga, J. Yeace. *Mater. Chem. A*, 2013, 1, 6664
- [41] B. Hammer and J. K. Norskov, *Surf. Sci.*, 1995, 343, 211–220.
- [42] S. Smidstrup, T. Markussen, P. Vancraeyveld, J. Wellendorff, J. Schneider, T. Gunst, B. Verstichel, D. Stradi, P. A Khomyakov, U. G Vej-Hansen, M-E. Lee et al, QuantumATK: an integrated platform of electronic and atomic-scale modelling tools, *J. Phys.: Condens. Matter* 32 (2020) 015901
- [43] J.P. Perdew, K. Burke, M. Ernzerhof, Generalized gradient approximation made simple, *Phys. Rev. Lett.* 77 (1996) 3865.
- [44] M.J. van Setten, M. Giantomassi, E. Bousquet, M.J. Verstraete, D.R. Hamann, X. Gonze, G.M. Rignanese, The PseudoDojo: Training and grading a 85 element optimized norm-conserving pseudopotential table. *Comput. Phys. Commun.* 226 (2018) 39–54,
- [45] Monkhorst, H. J. & Pack, J. D. Special points for Brillouin-zone integrations. *Phys. Rev. B* 13, 5188–5192 (1976).
- [46] L.G. Ferreira M. Marques, L.K. Teles Approximation to density functional theory for the calculation of band gaps of semiconductors, *Phys. Rev. B*, 78 (2008) 125116.
- [47] M. B. Kanoun, S. Goumri-Said, U. Schwingenschlogl, A. Manchon, magnetism in Sc-doped ZnO with zinc vacancies: A hybrid density functional and GGA+U approaches. *Chem. Phys. Lett.* 532 (2012) 96-99.
- [48] Tian, J. *Am. Chem. Soc* 2003, 125, 12384.
- [49] H. Chakhtouna, H. Benzeid, N. Zari, A. K. Qaiss, R. Bouhfid, Recent progress on Ag/TiO₂ photocatalysts: photocatalytic and bactericidal behaviors. *Environmental Science and Pollution Research*, 28, 44638–44666 (2021).
- [50] Rajakumar, A. Abdul Rauman, S. Mohana Roopan, V.G. Khanna, G. Elango, C. Kamaraj, A.A. Zahir, K. Velayutham, *Spectrochimica Acta Part A Molecular and Biomolecular Spectroscopy* 91:23-29, 2012.
- [51] K. Ashok Kumar, J. Manonmani, J. Senthilselvan, Effect on interfacial charge transfer resistance by hybrid co-sensitization in DSSC applications, *J Mater Sci: Mater Electron* (2014) 25:5296–5301.
- [52] E. H. Alsharaeh, T. Bora, A. Soliman, F. Ahmed, G. Bharath, M. G. Ghoniem, Khalid M. Abu-Salah, J. Dutta, Sol-Gel-Assisted Microwave-Derived Synthesis of Anatase Ag/TiO₂/GO Nanohybrids toward Efficient Visible Light Phenol Degradation, *Catalysts* 2017, 7, 133
- [53] Tsivadze, A., Ionova, G., Mikhalko, V., Ionova, I. and Gerasimova, G. (2013) Plasmon Properties of Silver Spherical Nanoparticles and Films. *Protection of Metals and Chemistry of Surfaces*, 49, 169-172.
- [54] J.K. Burdett, T. Hughbanks, G.J. Miller, J.W. Richardson, J.V. Smith, *J. Am. Chem. Soc.* 109, 3639 (1987)
- [55] M. Ikram, M. Wakeel, J. Hassan, A. Haider, S. Naz, A. Ul-Hamid, J. Haider, S. Ali, S. Goumri-Said, M. B. Kanoun, Impact of Bi Doping into Boron Nitride Nanosheets on Electronic and Optical Properties Using Theoretical Calculations and Experiments, *Nanoscale Res Lett* 16, 82 (2021)
- [56] M. Khan, J. Xu, N. Chen, W Cao, Asadullah, Z. Usman, D. F. Khan Effect of Ag doping concentration on the electronic and optical properties of anatase TiO₂: a DFT-based theoretical study, *Res Chem Intermed* (2013) 39:1633–1644
- [57] M. Guo, J. Du, First-principles study of electronic structures and optical properties of Cu, Ag, and Au-doped anatase TiO₂, *Physica B* 407 (2012) 1003–1007
- [58] Y. Wang, R. Zhang, J. Li, L. Li, S. Lin, First-principles study on transition metal-doped anatase TiO₂, *Nanoscale Res Lett* 2014, 9, 46
- [59] A Alshoaibi, M.B. Kanoun, B Ul Haq, S AlFaify, S Goumri-Said, Insights into the Impact of Yttrium Doping at the Ba and Ti Sites of BaTiO₃ on the Electronic Structures and Optical Properties: A First-Principles Study, *ACS Omega* 5, 15502-15509 (2020)